

# Inverse Design of High Absorption Thin-Film Photovoltaic Materials

Liping Yu,\* Robert S. Kokenyesi, Douglas A. Keszler, and Alex Zunger

## 1. Introduction

Enhancement of photocarrier collection by aiding drift through a very thin inorganic absorber film represents a promising route to new, high-efficiency photovoltaic (PV) devices.<sup>[1]</sup> The realization of such devices is largely predicated on the availability of materials that exhibit strong absorption across the solar spectrum with an abrupt onset at the band gap. Such materials have direct band gaps, but not all direct-band-gap materials are strong absorbers. Currently, ternary I-III-VI<sub>2</sub> chalcogenides, typified by CuInSe<sub>2</sub>, are among the strong direct band-gap absorbers known, establishing the basis for a commercial thin-film solar cell technology. While overall absorption is strong, the measured weak onset absorption near the band gap necessitates the use of rather thick films (~1.5 μm).<sup>[2]</sup> This thickness coupled with the relatively low abundance of In (In/Si = 10<sup>-7</sup>) potentially limits the scalability of this technology to the terawatt level.<sup>[3]</sup> Clearly, opportunities exist for advancing state-of-the-art thin-film PV through identification and design of new, strongly absorbing materials. However, there are currently no guiding rules (“design principles”) that reveal the physical factors distinguishing strong from moderate or weak direct-band-gap absorbers. In this work, we present a fundamental analysis of the factors that control absorption strength in compound semiconductors. From this analysis, we develop new insights into “absorption design principles”, propose candidate, highly absorbing materials, and experimentally assess their absorption properties.

Identification and design of the needed materials requires an approach beyond the classic one-dimensional Shockley-Queisser criterion,<sup>[4]</sup> which selects good PV absorbers solely on the basis of their band gap (direct or indirect) being in the range of 1.0–1.5 eV. This simple one-dimensional metric does not represent material-dependent optical absorption spectra and related radiative/nonradiative recombination losses, which are essential for evaluating a semiconductor as a thin-film absorber. Recently, we have proposed a new and improved

multi-dimensional metric, the so-called Spectroscopic Limited Maximum Efficiency (SLME), for the initial screening of candidate thin-film PV absorbers.<sup>[5]</sup> While neglecting extrinsic factors (such as dopability, metal contacts, etc.) in the initial stage of material screening, this metric depends explicitly on the calculated absorption spectrum and thickness of the thin-film absorber. It also accounts for the different types of optical transitions, i.e., direct allowed, direct forbidden, and indirect, near the absorption threshold. Our application of SLME<sup>[5]</sup> to ~300 ternary I-III-VI chalcogenide materials has revealed tens of candidates with SLME values comparable or higher than that of CuInSe<sub>2</sub>. We also use SLME to identify the underlying physical reasons for high absorption, so as to distill more general “absorption design principles”.

## 2. Initial Absorption-Strength Design Principles

We start by considering the channels of absorption in the known PV absorbers. (i) In binary semiconductors such as GaAs or CdTe the absorption at threshold occurs from the anion *p*-like valence band maximum (VBM) to the cation *s*-like conduction band minimum (CBM). (ii) In ternary chalcopyrites, i.e., Cu-III-VI<sub>2</sub> (III = Ga, In and VI = S, Se) containing *d*<sup>10</sup> Cu, the absorption at threshold benefits mostly from the transitions from (Cu-*d* + VI-*p*) near the VBM to (III-*s* + VI-*s*) near the CBM. Since the III-*s* band, (e.g. for In, near the CBM) is characterized by a rather wide dispersion,<sup>[6]</sup> it contributes to a broad density of states (DOS) and a rather slow rise of absorption with photon energy. In principle, the high dispersion near the CBM of chalcopyrites containing a group III element could be decreased, to the benefit of steeper absorption, by localizing the III *s* levels in a compound with a higher Cu/III ratio. This localization would lead to an increase in the DOS near the CBM and a corresponding enhancement of absorption. No compound of this type, however, is known.

This analysis suggests a few possible strategies for improvement. For example, the *s*-band narrowing at the CBM represents one potential strategy for tuning the absorption strength of materials related to Cu chalcopyrites. As another approach, we found from our SLME analysis of the I-III-VI system that when the element III is low-valence Tl<sup>1+</sup>, the compound exhibits higher SLME values than those containing high-valence Tl<sup>3+</sup> element. Whereas in CuInSe<sub>2</sub> with its high-valence In the (broadly dispersed) *s*-character is at the CBM, materials with low-valence Tl exhibit a considerable Tl *s*-like orbital density near the VBM and relatively flat *p*-like bands near the CBM. Since Cu *d*-like orbitals (high DOS) contribute mainly to the states near VBM, both *d* → *p* and *s* → *p* transitions contribute to an enhanced absorption strength in the Cu-Tl<sup>1+</sup>-VI compounds. Hence, Cu

Dr. L. Yu, Prof. A. Zunger  
University of Colorado Boulder  
Colorado 80309, USA  
E-mail: yuliping@gmail.com

Dr. R. S. Kokenyesi, Prof. D. A. Keszler  
Department of Chemistry  
Oregon State University  
153 Gilbert Hall, Corvallis, Oregon 97331-4003 USA

Dr. L. Yu  
National Renewable Energy Laboratory  
Golden, Colorado 80401, USA



DOI: 10.1002/aenm.201200538

chalcogenides containing low-valence ions with an  $ns^2$  electron configuration appear to be promising systems for realization of very high absorption coefficients.

Having understood this principle, we can proceed to materials that embody this principle without the toxic and scarce elements Tl and In. We have chosen to consider the system Cu-V-VI ( $V = P, As, Sb, Bi$ ;  $VI = S, Se$ ). Group V elements adopt two common oxidation states, namely  $5+$  and  $3+$ , with valence electron configurations  $s^0p^0$  and  $s^2p^0$ , respectively, mirroring the two configurations of the Group III elements (e.g.,  $Tl^{3+}s^0p^0$  and  $Tl^{1+}s^2p^0$ ). Compounds with high Cu/V $^{5+}$  ratios are known, providing an opportunity to examine the effects of high DOS  $s$ -orbital contributions near the CBM on the absorption strength. In addition, the low-valence compounds can be studied with respect to the enhancement of absorption through the  $s$ -like VBM to  $p$ -like contributions near the CBM.

To this end, we have calculated the band gaps, absorption spectra and SLME values for the 30 Cu-V-VI materials listed in Table S1 that have been reported in the inorganic crystal structure database (ICSD).<sup>[7]</sup> We identify important trends in absorption strength on the basis of projected  $s, p$  DOS near the band edges to examine our initial design assumptions. We have also used the ensuing theory-derived design principles to guide initial experiments, allowing us to propose candidate, very thin absorber films for enhancing PV efficiency. The process opens expanded opportunities beyond the Shockley-Queisser construct for identifying new absorbers and motivating their development.

### 3. Calculated Absorption Spectra

The density functional theory (DFT) approach has systematic errors in depicting a material's excited properties such as band gap and absorption spectrum, predominantly due to its failure to remove the unphysical interaction of electron with itself. The present calculations, based on the GW approximation<sup>[8]</sup>

for the electron's self-energy, which includes, in addition to DFT-like terms in the Hamiltonian, also a non-local self energy operator which greatly improves the description of correlation. Out of many GW schemes, we choose to apply GW approximation perturbatively on the top of the wave functions and energy eigenvalues calculated from a generalized Kohn-Sham scheme with the hybrid exchange-correlation functional HSE06,<sup>[9]</sup> i.e.,  $G_0W_0@HSE06$ .<sup>[10]</sup> Within this scheme, it has been shown that for a variety of materials (even those with shallow  $d$  states), the calculated excited-state properties such as band gaps agree well with experiment.<sup>[10,11]</sup>

Within the Cu-V-VI system, there are four element sets, namely, Cu-As-S, Cu-As-Se, Cu-Sb-S, and Cu-Sb-Se, each having compositions with both low valence  $V^{3+}$  and high valence  $V^{5+}$ . **Figure 1** shows the comparison of the calculated optical absorption spectra above their respective minimum band gaps between Cu- $V^{3+}$ -VI and Cu- $V^{5+}$ -VI compounds within these four element sets. It is seen that the low-valence Cu- $V^{3+}$ -VI compounds consistently exhibit the higher absorption coefficients at photon energies  $h\nu > E_g + \delta$ , where  $\delta$  is zero or some finite positive value less than about 1 eV. The high valence Cu- $V^{5+}$ -VI compounds are also found to have stronger absorption than high valence CuIn $^{3+}$ Se $_2$  within some energy range above (but not too far away from) their respective  $E_g$ . We shall show later that this  $\delta$  depends on the energy distance (denoted here as  $\Delta$  for convenience) from  $E_g$  to the dipole-allowed direct band gap of the compared materials.

### 4. Analysis of Orbital Contributions Near VBM and CBM

To identify the atomic orbital contributions in the compound near the VB or CB edges, we calculate the angular momentum  $l$  projected DOS per volume, integrated within an energy range of  $\eta$  from the VBM ( $E_v$ ) or CBM ( $E_c$ ) respectively. For an orbital with angular momentum  $l$  ( $s, p, \dots$ ), this quantity can be written as

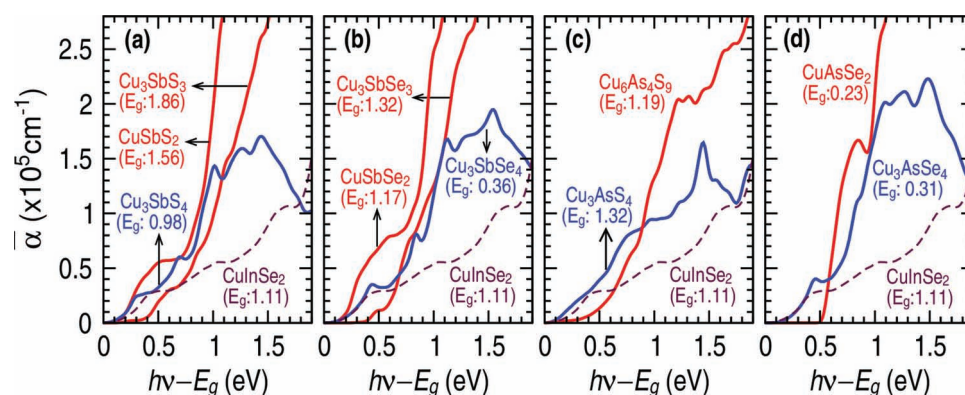


**Figure 1.** Calculated optical absorption spectra for Cu- $V^{5+}$ -VI compounds (blue) and Cu- $V^{3+}$ -VI compounds (red) within the element sets of (a) Cu-Sb-S, (b) Cu-Sb-Se, (c) Cu-As-S, and (d) Cu-As-Se using the first principles quasi-particle GW method based on wavefunctions generated from hybrid functional HSE06. CuInSe $_2$  (dashed) is shown as reference. Minimum band gaps ( $E_g$ ) are aligned at  $E = 0$ . The energy differences ( $\Delta$ ) between  $E_g$  and dipole-allowed direct gaps for the indirect materials are CuSbS $_2$  (0.05 eV), Cu $_3$ SbS $_3$  (0.13 eV), CuSbSe $_2$  (0.09 eV), Cu $_3$ SbSe $_3$  (0.26 eV), and CuAsSe $_2$  (0.55 eV).

$$I_{DOS}^v(\eta) = \frac{1}{\Omega} \int_{E_v-\eta}^{E_v} \rho_l(E) dE, \text{ or } I_{DOS}^c(\eta) = \frac{1}{\Omega} \int_{E_c}^{E_c+\eta} \rho_l(E) dE \quad (1)$$

where  $\rho_l(E) = \sum_{\alpha} \rho_l^{\alpha}(E)$  where  $\rho_l^{\alpha}(E)$  is the  $l$ -projected DOS of atom  $\alpha$  which runs over all atoms of interest in the unit cell of volume  $\Omega$ . We choose  $\eta = 2.0$  eV, which effectively covers solar photon absorption for a material with  $E_g$  near 1 eV. The calculated  $s$ ,  $p$  integrated DOS contributions of group V atoms near the band edges of 19 compounds are summarized in Figure 2a ( $s_{DOS}^v$  and  $s_{DOS}^c$ ) and Figure 2b ( $p_{DOS}^v$  and  $p_{DOS}^c$ ). One can see that the contributions of  $s$  and  $p$  orbitals of group V atoms in low valence Cu-V<sup>3+</sup>-VI compounds are different from that of high valence Cu-V<sup>5+</sup>-VI compounds. Specifically, three clear trends<sup>[12]</sup> are found: (i) The  $s$ -like orbital contribution of group V atoms in the high-valence Cu-V<sup>5+</sup>-VI compounds is larger in CB states than that in VB states, while in low-valence Cu-V<sup>3+</sup>-VI compounds such  $s$ -orbital contribution are dominant in the VB states over the CB states. (ii) The  $p$ -like orbital contributions of group V atoms in the low-valence Cu-V<sup>3+</sup>-VI are higher than that in the high-valence Cu-V<sup>3+</sup>-VI near both VBM and CBM. (iii) The  $p$ -like orbitals contribution of group V atoms in the low-valence compounds is much higher near CBM than VBM.

## 5. Relationship Between Orbital Character of DOS and Absorption Spectra

In Cu-V<sup>5+</sup>-VI materials the  $s$ -like orbital states around the high valence group V atoms near the CBM mirrors the  $s$ -like character around the high valence group III atoms (In) near the CBM of CuInSe<sub>2</sub>. Since the considered all high-valence V<sup>5+</sup> atoms have smaller ionic radii than In<sup>3+</sup> and larger oxidation state number, they are more diluted in both volume and composition, which leads to slightly less  $s$ -orbital contributions near CBM (see Figure 2a). However, on the other hand, the V<sup>5+</sup> atoms have two more  $p$  electrons than In<sup>3+</sup> atoms, and the smaller ionic radii (shorter V-VI bonds, stronger electrostatic interaction) push more V-derived  $p$ -orbital contribution into bands near CBM (see Figure 2b), which translates into a higher  $p$ -DOS near the CBM, a higher joint DOS, and enhanced absorption relative to CuInSe<sub>2</sub>.

In materials with low-valence V<sup>3+</sup> atoms,  $p$ -like orbitals around V contribute significantly near the CBM and the VBM, while  $s$ -like states are more pronounced near the VBM. This picture of the electronic structure is consistent with that commonly associated with the  $ns^2$  electron configuration, e.g., low-valence group V atoms, and the stereochemical activity of "lone pair" electrons.<sup>[13]</sup> This activity is manifest in the highly asymmetric coordination environments of the V<sup>3+</sup> atoms. In these distorted environments, there is a de-mixing of a portion of the V  $p$ -like and VI  $p$ -like bonding orbitals. The dispersion of the V  $p$ -like states then flatten relative to those of a high-valence V atom occupying a structurally symmetric site. This reduced dispersion then results in a high DOS near CBM. The same considerations apply to the high  $s$ -like DOS near the VBM. In the ternary Cu-M-VI compounds, Cu  $d$ -like orbitals with high DOS are concentrated near the VBM, so generally both electric

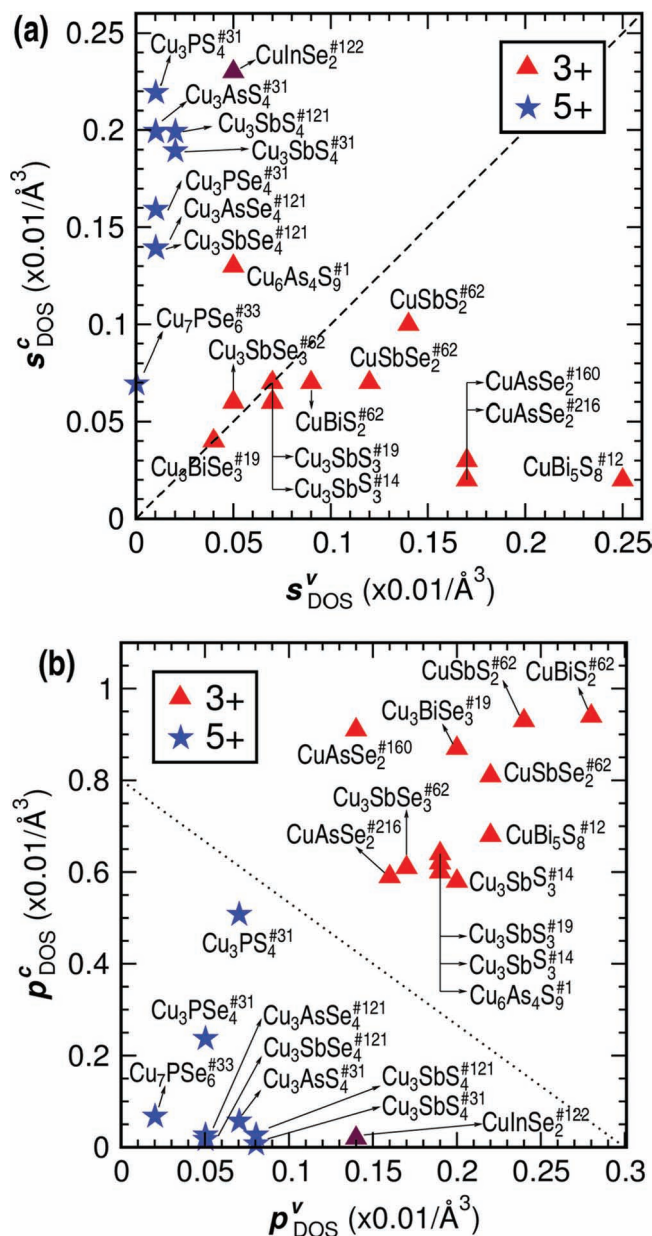


**Figure 2.** Integrated DOS per volume within 2.0 eV of band edges (see Equation (1) for (a)  $s$ -orbitals in valence and conduction bands, and (b)  $p$  orbitals in valence and conduction bands of group V atoms in the text). CuInSe<sub>2</sub> is shown for comparison. The superscript over the chemical formula corresponds to the space group number of the corresponding compound. The dashed diagonal line in (a) indicates  $s_{DOS}^c(2\text{ eV}) = s_{DOS}^v(2\text{ eV})$  emphasizing that the high-valence V atom has dominant  $s$  character at the CBs while the low-valence atom has predominantly  $s$  character at the VBs. The dotted line in (b) emphasizes that the low-valence V atoms have more  $p$ -like orbital contributions near both band edges than high-valence ones (see text for details).<sup>[12]</sup>

dipole-allowed Cu  $d \rightarrow Vp$  and  $Vs \rightarrow Vp$  transitions should contribute to a strong absorption. The less dispersive band character near both the VBM and CBM thus contributes to a high joint DOS, making the low-valence Cu-V-VI materials exceptionally strong absorbers.

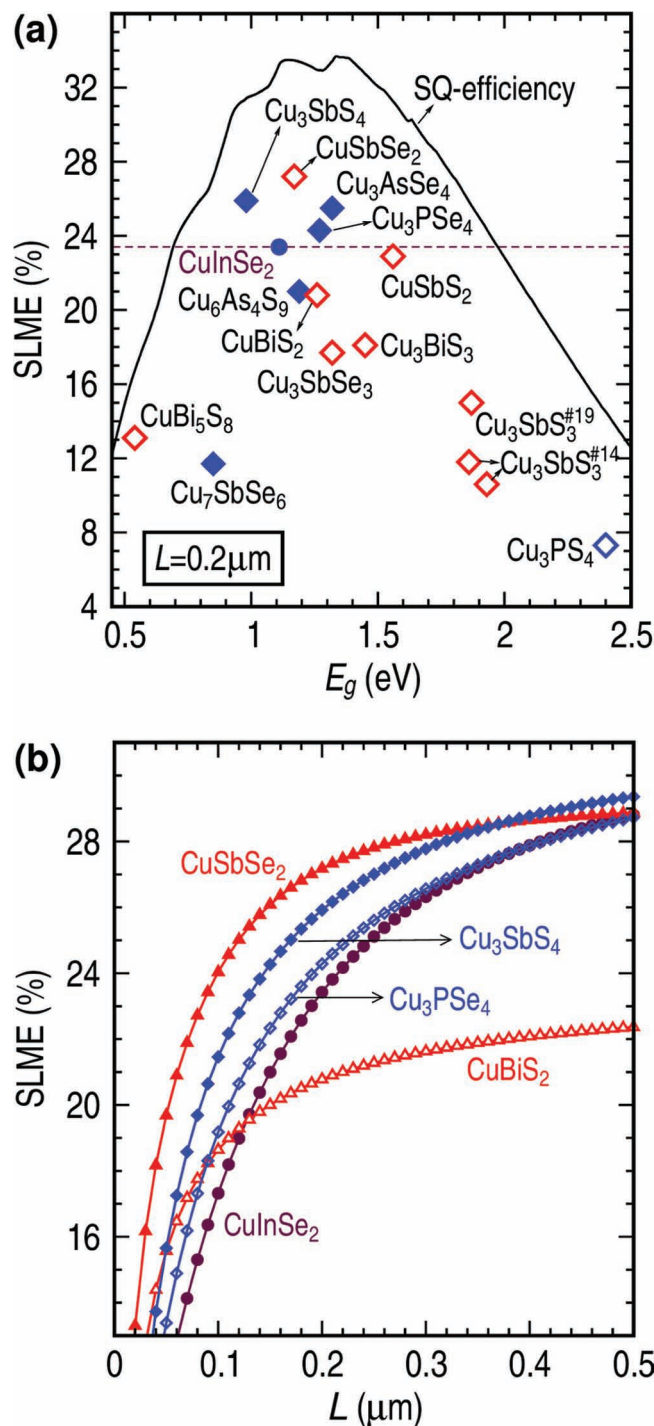
These considerations, however, must be tempered by the nature of the band gap, i.e., direct vs. indirect. For example,  $\text{CuSb}^{3+}\text{S}_2$  is an indirect band gap material with a very small  $\Delta$  value (i.e., the energy difference between indirect gap and dipole-allowed direct gap  $\Delta = 0.05$  eV). As seen from Figure 1(a), in comparison with the direct-gap materials  $\text{Cu}_3\text{Sb}^{3+}\text{S}_4$  and  $\text{CuInSe}_2$ ,  $\text{CuSbS}_2$  has stronger absorption strength for photons with  $h\nu > E_g + \delta$ , where  $\delta \approx 0$ . For  $\text{Cu}_3\text{SbS}_3$ , however, where Sb is also in the low-valence state, the absorption becomes stronger than  $\text{CuInSe}_2$  and  $\text{Cu}_3\text{SbS}_4$  only when  $h\nu > E_g + \delta$  with  $\delta > 0.7$  eV. Here, a larger difference ( $\Delta = 0.13$  eV) exists between the indirect gap and the dipole-allowed direct gap. This larger  $\Delta$  means that the absorption coefficient only begins to rise rapidly at an energy near the direct optical transition above  $E_g$ . The optical absorption near threshold for a material with large  $\Delta$  will generally be much weaker than that in a material with very small (or zero)  $\Delta$ .

## 6. Spectroscopic Limited Maximum Efficiency Results and Their Correlation to Absorption Strength

A strong optical absorption above a suitable  $E_g$  is a necessary condition for realizing highly efficient, thin-film PV performance.<sup>[14]</sup> Calculated SLME values at a film thickness of 200 nm for 15 Cu-V-VI materials with  $E_g$  between 0.5 and 2.5 eV are shown in Figure 3a. Seven of the compounds, namely,  $\text{CuSbS}_2$ ,  $\text{CuSbSe}_2$ ,  $\text{Cu}_3\text{SbS}_4$ ,  $\text{Cu}_3\text{PSe}_4$ ,  $\text{Cu}_3\text{AsSe}_4$ ,  $\text{Cu}_6\text{As}_4\text{S}_9$ , and  $\text{CuBiS}_2$ , are found to have comparable or higher SLME (>20%) than  $\text{CuInSe}_2$ . The modeled film thickness is approximately eight times thinner than that commonly found in  $\text{CuInSe}_2$ -type PV cells. As seen in Figure 3b, the SLME metric provides a unique assessment of efficiency as a function of film thickness. Clearly, those materials with high absorption coefficients and rapid onsets near threshold, cf., Figure 1 and Figure 3, exhibit the higher efficiencies. They provide unique opportunities for examining cell performance with absorber layers much thinner than those commonly used in current thin-film PV technologies.

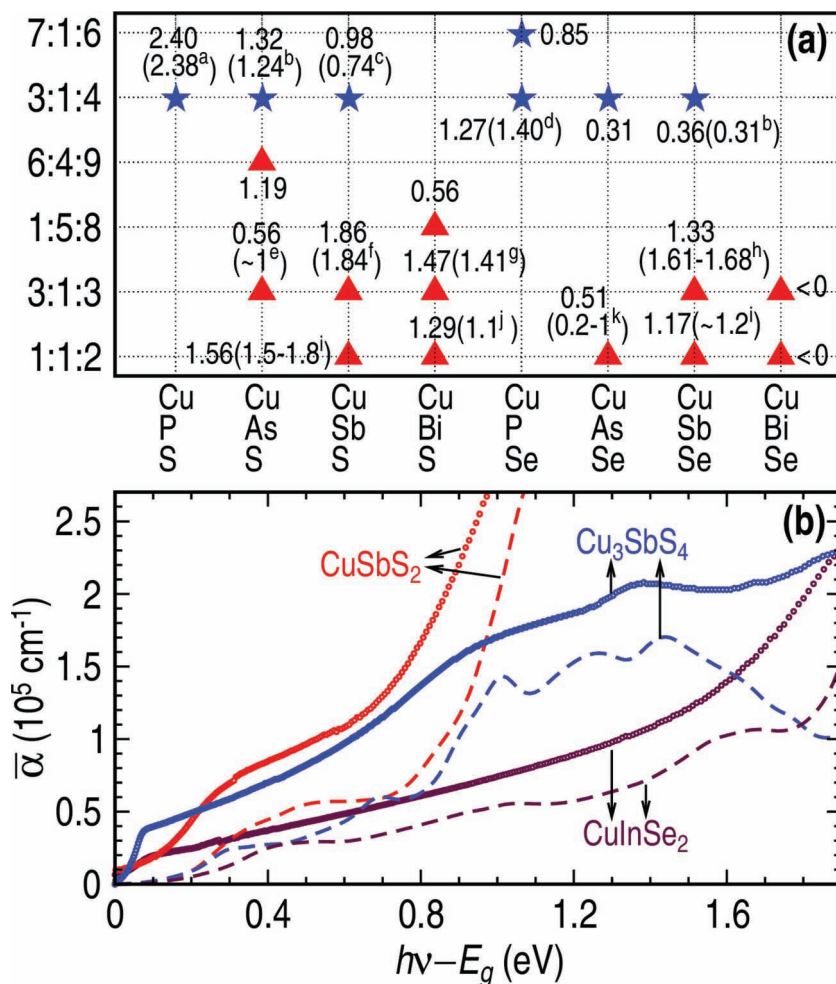
## 7. Comparison of Theory and Experiment

Figure 4a summarizes our calculated band gaps ( $E_g$ ) for 19 Cu-V-VI compounds distributed across six distinct compositions, deviating by an average of 0.15 eV from experimentally determined values (good agreement). Figure 4b shows the comparison of absorption coefficients between theory and experiment for the materials  $\text{Cu}_3\text{SbS}_4$ ,  $\text{CuSbS}_2$ , and  $\text{CuInSe}_2$  as shown Figure 1a. Consistent with the computed assessment, the Sb compounds are found to have much higher absorption than  $\text{CuInSe}_2$ . Similarly, as predicted,  $\text{CuSbS}_2$  is found to have the highest overall absorption above threshold. A better agreement between experiment and theory can be also seen if we shift the experimental absorption coefficient curves by about  $-0.2$  eV. In other words, the theoretical absorption strength near the threshold is universally underestimated. For  $\text{Cu}_3\text{SbS}_4$  and  $\text{CuSbS}_2$ , one can see that the measured absorption



**Figure 3.** (a) Calculated SLMEs for group Cu-V-VI materials and (b) SLME vs film thickness for selected high-efficiency materials. The open (filled) symbols in (a) represent indirect (direct) band gap materials. In both (a) and (b), red (blue) color denotes for the Cu-V-VI compounds low (high)-valence Group V element.

coefficient rises above  $10^5$   $\text{cm}^{-1}$  at approximately 0.5 eV above threshold, while the related absorption reaches the same level only at 0.8 eV above threshold. This might be expected since the excitonic effects and phonon-assisted transitions that also contribute to the absorption near the threshold are neglected



**Figure 4.** (a) Calculated  $G_0W_0$  band gaps (in eV) for  $\text{Cu-V}^{3+}\text{-VI}$  (red triangles) and  $\text{Cu-V}^{5+}\text{-VI}$  (blue stars) materials ( $V = \text{P, As, Sb, Bi}$  and  $\text{VI} = \text{S, Se}$ ). The available experimental gaps are shown in parenthesis, and corresponding references are indicated by the superscript letters, i.e., a,<sup>[15]</sup> b,<sup>[16]</sup> c,<sup>[17]</sup> d,<sup>[18]</sup> e,<sup>[19]</sup> f,<sup>[20]</sup> g,<sup>[21]</sup> h,<sup>[22]</sup> i,<sup>[23]</sup> j,<sup>[24]</sup> and k.<sup>[25]</sup> (b) Experimental (circles) and calculated (dashed lines, same as in Figure 1a) absorption coefficients for  $\text{CuSbS}_2$  (red),  $\text{Cu}_3\text{SbS}_4$  (blue), and  $\text{CuInSe}_2$  (maroon) thin films. The optical band gaps extracted from our experiments are 1.44, 0.88, and 1.03 eV, respectively.

in the calculations. On the other hand, the experimental measured absorption may also contain the contribution from sub-gap effects (e.g., due to defects or surfaces) in the thin film, which are not considered in the calculations. The measured band gap values may also have some deviations due to the non-parabolic behavior near the band edges.

While  $\text{CuSbS}_2$  exhibits very strong absorption, its SLME value (23%) for a 200-nm thick film is surpassed by other members of the  $\text{Cu-V-VI}$  family. Its indirect band gap at 1.44 eV (Table S2) and delayed rapid onset at  $E_g + 0.14$  eV slightly compromises absorption in a critical portion of the solar spectrum, which would limit performance in very thin devices.<sup>[26]</sup> From electrical measurements, we estimate a rather low hole carrier mobility (0.1  $\text{cm}^2/\text{Vs}$ ) in  $\text{CuSbS}_2$  (Table S2), although a value nearly an order of magnitude higher has been reported in  $\text{CuSbSe}_2$  thin films,<sup>[27]</sup> where  $\text{CuSbSe}_2$  has the highest SLME value in Figure 3.

The materials of composition  $\text{Cu}_3\text{-V-VI}_4$  ( $V = \text{P, As, Sb}$ ) also have SLME values higher than that of  $\text{CuInSe}_2$  for films thinner than 300 nm. As shown in Table S2, this family also offers numerous opportunities for compositional tuning of band gaps across the range from  $\text{Cu}_3\text{SbSe}_4$  (0.6 eV) to  $\text{Cu}_3\text{PS}_4$  (2.4 eV). At the same time, high hole mobility (1–15  $\text{cm}^2/\text{Vs}$ ) and low carrier concentrations ( $\sim 10^{16}/\text{cm}^3$ ) are readily realized in pressed pellets and thin films (Table S2). These electrical properties make these materials especially promising with respect to thin-film PV, as they indicate grain boundaries may be rather benign with respect to carrier recombination. Hence, the  $\text{Cu}_3\text{-V-VI}_4$  family provides new opportunities for the development of high-efficiency thin-film solar cells in a variety of configurations.<sup>[28]</sup>

## 8. Summary and Outlook

Some potential Cu-based thin film PV absorber materials have been identified using an inverse design approach. Specifically, (i) we first set upfront the property to be addressed (here, solar absorption); (ii) then we apply SLME metric that reflects the target property to search over a large space of compounds based on first principles quasi-particle calculations; (iii) having found promising candidates, we next select a well-defined set of materials for detailed experimental and further theoretical examination. In this inverse way we thus avoid unconstrained studies of countless compounds for PV absorber applications.

We conclude that rapid onset to high absorption above the band gap in Cu-M-VI ( $M = \text{group III-V}$ ) materials can be achieved by i) including M elements in  $s^2p^0$  low-valence electronic configuration, or ii)  $\text{Cu}/M > 1$  cation stoichiometry. High absorption in materials

containing low-valence V atoms arises from allowed transitions and high joint DOS derived from relatively flat V s-like and Cu d-like bands near VBM and V p-like bands near CBM. These factors are plainly displayed by the high SLME value (27%) for the indirect band-gap material  $\text{CuSbSe}_2$ . An even higher SLME should be observed in a direct-gap material containing a low-valence group V atom. High absorption in materials containing high-valence V atoms arises from a high joint DOS associated with structural localization giving rise to relatively flat V s-like bands near VBM. These semiconductor absorbers are well represented by the family  $\text{Cu}_3\text{-V-VI}_4$ , which contains many members exhibiting SLMEs > 23% at a film thickness of 200 nm. This inherent efficiency, coupled with tunable band gaps, useful electrical properties, and low fabrication temperatures, makes this family of materials especially attractive as candidates for investigation and development of new single-junction

and tandem solar cells. Developing an understanding of the fundamental factors driving strong absorption in the Cu-V-VI materials has provided new insight, refining and focusing design pathways for discovery of improved materials.

## 9. Experimental Section

**Calculations:** The first principles calculations presented here were carried out by using the VASP code,<sup>[29]</sup> PAW potentials.<sup>[30,31]</sup> An energy cutoff of 300 eV is chosen. For each material, the atomic positions are fully relaxed by HSE06 while lattice parameters were kept fixed to experimental ones. In GW band gap calculations, we have used the  $\Gamma$ -centered homogeneous  $k$ -meshes ( $k_1 \times k_2 \times k_3$ ) which are determined according to the sizes of lattice vectors ( $\vec{a}_1, \vec{a}_2, \vec{a}_3$ ), i.e.,  $k_i = 8, 6, 4, 2, 1$  respectively for  $|\vec{a}_i| \leq 4.5 \text{ \AA}$ ,  $4.5 \text{ \AA} < |\vec{a}_i| \leq 7.5 \text{ \AA}$ ,  $7.5 < |\vec{a}_i| \leq 9.5 \text{ \AA}$ ,  $9.5 \text{ \AA} < |\vec{a}_i| \leq 16 \text{ \AA}$ ,  $|\vec{a}_i| > 16 \text{ \AA}$ , where  $i = 1, 2, 3$ . The number of unoccupied bands in GW band gap calculation is at least nine times of the number of occupied bands for a system with fewer than 40 atoms. For larger system that can be handled, we use  $\sim 1280$  total bands that usually contains at least 512 unoccupied bands.

For optical absorption spectrum calculations, we used HSE06 plus scissor operator, i.e., the quasiparticle energies are computed by shifting these HSE06 eigenvalues of the conduction bands by a scissor operator. The number of empty bands used here is about 3-4 times the number of the occupied bands. The density of  $k$ -point mesh chosen here doubles the one used in GW band gap calculations for the respective material. In all calculations, the spin-orbit coupling, photon-assisted absorption, and excitonic effects are not considered in this work.

**Experiments:** Bulk synthesis was carried out using stoichiometric mixtures of high-purity (99.99%) elements annealed in the 450–550 °C temperature range in evacuated sealed fused-silica tubes. Cu and Sb<sub>2</sub>S<sub>3</sub> thin layers of appropriate thicknesses were deposited onto SiO<sub>2</sub> substrates by electron-beam evaporation and then annealed at 300 °C for 30 min in the presence of sulfur to obtain single phase CuSbS<sub>2</sub> and Cu<sub>3</sub>SbS<sub>4</sub>. Phase purity of bulk and thin-film samples was evaluated on a Rigaku Ultima-IV X-ray diffractometer. Thin-film optical transmission and reflectance spectra were measured by using an Oriel grating spectrometer with a W-lamp source. Diffuse reflectance spectra of powders were obtained by using an Ocean Optics UV-vis-IR setup followed by analysis via the Kubelka-Munk method.<sup>[32]</sup> Electrical properties were measured on polycrystalline thin films and bulk pressed pellets in the van der Pauw configuration on a Lakeshore (Model 7504) Hall measurement system.

## Supporting Information

Supporting Information is available from the Wiley Online Library or from the author.

## Acknowledgements

This work was supported by U.S. DOE, Office of Science, Energy Frontier Research Centers, and used capabilities of the NREL Computational Sciences Center supported by U.S. DOE EERE, under Grant No. DEAC36-08GO28308 to NREL. The "Center for Inverse Design" is a DOE Energy Frontier Research Center.

Received: July 17, 2012

Published online: August 27, 2012

- [1] A. Rose, *Phys. Stat. Sol. A* **1979**, 56, 11.
- [2] W. N. Shafarman, L. Stolt, in *Handbook of Photovoltaic Science and Engineering*, (Eds: A. Luque, S. Hegedus), John Wiley & Sons Ltd, West Sussex, UK, Ch. 13.
- [3] C. S. Tao, J. Jiang, M. Tao, *Sol. Energ. Mat. Sol. C.* **2011**, 95, 3176.
- [4] W. Shockley, H. J. Queisser, *J. Appl. Phys.* **1961**, 32, 510.
- [5] L. Yu, A. Zunger, *Phys. Rev. Lett.* **2012**, 108, 068701.
- [6] J. E. Jaffe, Alex Zunger, *Phys. Rev. B* **1984**, 29, 1882.
- [7] F. Karlsruhe, "Inorganic Crystal Structure Database," <http://www.fiz-karlsruhe.de/icsd.html> (accessed August, 2012).
- [8] L. Hedin, *Phys. Rev.* **1965**, 139, A796.
- [9] J. Heyd, G. E. Scuseria, M. Ernzerhof, *J. Chem. Phys.* **2006**, 124, 219906.
- [10] F. Fuchs, J. Furthmüller, F. Bechstedt, M. Shishkin, G. Kresse, *Phys. Rev. B* **2007**, 76, 115109.
- [11] C. Rödl, F. Fuchs, J. Furthmüller, F. Bechstedt, *Phys. Rev. B* **2009**, 79, 235114.
- [12] Note that the  $l$ -projected DOS of a group V atom  $\alpha$  (i.e.,  $\rho_l^\alpha(E)$ ) is calculated with a fixed spherical radius, i.e., independent of its valence state. Physically, the  $V^{3+}$  atom has a larger ionic radius than  $V^{5+}$ . Using larger radii for  $V^{3+}$  atoms, the calculated  $S_{DOS}^{V,C}$  and  $P_{DOS}^{V,C}$  are actually larger, i.e., the 'red triangles' in both (a) and (b) shifting up and right, which makes the observed trends here more robustly.
- [13] A. Walsh, D. J. Payne, R. G. Egdell, G. W. Watson, *Chem. Soc. Rev.* **2011**, 40, 4455.
- [14] L. Yu, S. Lany, R. K. Kykyneshi, V. Jieratum, B. Pelatt, E. Altschul, H. A. S. Platt, J. F. Wager, D.A. Keszler, A. Zunger, *Adv. Energy Mater.* **2011**, 1, 748.
- [15] J. V. Marzik, A. K. Hsieh, K. Dwight, A. Wold, *J. Solid State Chem.* **1983**, 49, 43.
- [16] L. I. Berger, V. D. Prochukhan, *Ternary Diamond-like Semiconductors*. New York, London: Consultants Bureau, **1969**.
- [17] *Handbook of Chemistry and Physics*, (Ed: D. R. Lide), Chemical Rubber Company, Boca Raton, FL, 76th edition, **1995–96**.
- [18] D. H. Foster, V. Jieratum, R. Kykyneshi, D. A. Keszler, G. Schneider, *Appl. Phys. Lett.* **2011**, 99, 181903.
- [19] J. H. Wernick, US patent no. 2882193, **1959**.
- [20] P. Maiello, G. Zoppi, R. Miles, N. Pearsall, I. Forbes, in *The 7th Photovoltaic Science Applications and Technology Conference and Exhibition (PVSAT-7)* Edinburgh, Scotland, **2011**, 65.
- [21] F. Mesa, G. Gordillo, *J. Phys., Conf. Ser.* **2009**, 167, 012019.
- [22] A. Bansal, T. Deutsch, J. E. Leisch, S. Warren, J. A. Turner, A. M. Fernandez, *Proceedings of the 2001 U.S. DOE Hydrogen Program Review* Baltimore, Maryland, **2001**, pages: 347–358.
- [23] D. Colombara, L. M. Peter, K. D. Rogers, J. D. Painter, S. Roncallo, *Thin Solid Films* **2011**, 519, 7438.
- [24] S. H. Pawar, A. J. Bhosale, P. N. Pawar, *Bull. Mater. Sci.* **1986**, 8, 423.
- [25] J. H. Wernick, K. E. Benson, *J. Phys. Chem. Solids* **1957**, 3, 157.
- [26] Y. Rodriguez-Lazcano, M. T. S. Nair, P. K. Nair, *J. Electrochem. Soc.* **2005**, 152, G635.
- [27] D. Tang, J. Yang, F. Liu, Y. Lai, M. Jia, J. Li, Y. Liu, *Electrochem. Solid St. Lett.* **2012**, 15, D11.
- [28] A. De Vos, *J. Phys. D: Appl. Phys.* **2012**, 13, 83946.
- [29] G. Kresse, J. Furthmüller, *Phys. Rev. B* **1996**, 54, 11169.
- [30] P. E. Blochl, *Phys. Rev. B* **1994**, 50, 17953.
- [31] G. Kresse, D. Joubert, *Phys. Rev. B* **1999**, 59, 1758.
- [32] P. Kubelka, F. Munk, *Zeit. Für Techn. Physik* **1931**, 12, 593.